ジットナノ粒子，ハイブリッドナノ粒子，ポリマーミセル，ポリマー抱合体)と複数の抗がん剤，siRNA，miRNA などを組み合わせることにより治療抵抗性に打ち勝つと考えられ，*in vivo* 系での研究成果が発表されている[10,11]．Apt-conjugated thermally cross-linked SPION や PSMA(Prostate-specific membrane antigen)Apt-conjugated Gold NP は，MRI 画像診断およびドキソルビシンを組み合わせることで前立腺がん治療への応用をめざしている[10,11]．

前立腺がん細胞におけるドセタキセルと Fe_3O_4磁性体ナノ粒子の併用効果

本研究室で行った Fe_3O_4磁性体ナノ粒子併用による DTX の効果についての基礎的実験を一部紹介する[12]．

1. Fe_3O_4磁性体ナノ粒子の前立腺がんへの影響

使用した Fe_3O_4磁性体ナノ粒子の一次粒子径は約 10 nm で，培養液中において凝集する二次粒子径は 208.6±49.1 nm であった．Fe_3O_4磁性体ナノ粒子(10 μg/mL)を前立腺がん細胞株 DU145 に曝露し，透過電子顕微鏡(transmission electron microscopy：TEM)でナノ粒子の細胞内取込みを確認した(図 2)．前立腺がん細胞株 DU145，LNCaP，前立腺由来間質細胞株 PrSC に Fe_3O_4 磁性体ナノ粒子を曝露したが，LNCaP は濃度依存的に細胞生存率の低下を認めた．

つぎに活性酸素種(reactive oxygen species：ROS)の測定を行った．LNCaP に比べて，DU145 における ROS 産生は用量依存的に増加し，Fe_3O_4 磁性体ナノ粒子の曝露濃度 100 μg/mL では H_2O_2 曝露(100 μM)と同程度の ROS 産生を認めた(図 3)．LNCaP の場合，濃度 100 μg/mL の Fe_3O_4磁性体ナノ粒子の処理時のみ ROS の有意な増加を認めた．また酸化ストレスマーカーのひとつである 8-hydroxy-2'-deoxyguanosine(8-OHdG)産生の測定を行った．それぞれの株における 8-OHdG のレベルは用量依存的に増加するのを認めた．

2. ドセタキセルに磁性体ナノ粒子の併用による効果

前立腺がん細胞株 DU145 および LNCaP に DTX と Fe_3O_4磁性体ナノ粒子を曝露し，細胞生存率およびアポトーシスを測定した．両細胞株において，Fe_3O_4 磁性体ナノ粒子の曝露濃度 100 μg/mL 併用にて DTX の効果を高めた(図 4)．

3. まとめ

Fe_3O_4磁性体ナノ粒子は食作用，飲作用，非特異的エンドサイトーシスなどのエンドサイトーシスの機構を介して細胞内に侵入し，その後リソソームなどに蓄積し，細胞内で ROS を産生したと考えられる．この DU145 における ROS 産生は二酸化チタンやフラーレンなどのナノマテリアルを曝露したときには認められなかった[13]．すでに酸化鉄磁性材料は MRI 造影剤の主成分として人体内への導入する薬事承認を受けているが，細胞毒性が細胞の種類により異なるなどの潜在的な毒性が報告されている．とくに前立腺がんの酸化ストレスはその発生・進展に関与し，その取扱い方は諸刃の剣であるが，治療へつながると考えられている[14]．Fe_3O_4磁性体ナノ粒子(曝露濃度 100 μg/mL)の併用により DTX の効果の増強を認めた．この増強メカニズムにはミトコンドリア膜障害や ER ストレスなどが関与すると考えている．この増強はかならずしも十分ではないが，温熱による抗がん剤感受性の向上(thermal-sensitivity)あるいは温熱療法(thermo-chemotherapy)との併用により[15]，DTX の副作用を減らしつつ，治療効果を向上の能性を示したと考えられる．

今後は，前立腺がん標的指向性 Fe_3O_4磁性体ナノ粒子を中心としたセラノスティクスのさらなる研究が必要である．

謝辞：これらの研究は JSPS 科研費 24592379 の助成を受けたものです．また，横浜市立大学大学院医学部泌尿器科教室・上村博司先生，神奈川科学技術アカデミー光触媒グループ・石黒　斉先生，産業医大職業性腫瘍学教室・河井一明先生のご協力をいただきましたことを，ここに深謝いたします．

文献

1) Jain, K. K.：Advances in the field of nanooncology. *BMC Med.*, **8**：83, 2010.
2) Ahmed, N. et al.：Theranostic applications of nanoparticles in cancer. *Drug Discov. Today*, **17**-

18：928-934, 2012.
3) 中川　貴・他．磁性体ナノ粒子のバイオ・医療応用の最新動向．電気学会全国大会講演論文集，**2**：S4(4)-S4(7)，2011.
4) Singh, A. et al.：Magnetic nanoparticles：a novel platform for cancer theranostics. *Drug Discov. Today*, **19**：478-481, 2014.
5) Mahmoudi, M. et al.：Superparamagnetic iron oxide nanoparticles(SPIONs)：development, surface modification and applications in chemotherapy. *Adv. Drug Deliv.*, **63**：24-46, 2011.
6) Tabata, N. et al.：Partial cancer prevalence in Japan up to 2020：estimates based on incidence and survival data from population-based cancer registries. *Jpn. J. Clin. Oncol.*, **38**：146-157, 2008.
7) Watanabe, M. et al.：Comparative studies of prostate cancer in Japan versus the United States. A review. *Urol. Oncol.*, **5**：274-283, 2000.
8) 塩田真己・他：去勢抵抗性前立腺癌の成因と新規治療の展望．福岡医学雑誌，**103**：91-97，2012.
9) Schweizer, M. T. et al.：Chemotehrapy and its evoving role in the management of advanced prostate cancer. *Asian J. Androl.*, **16**：334-340, 2014.
10) Sanna, V. et al.：Nanoparticle therapeutics for prostate cancer treatment. *Nanomedicine*, **8**：S31-S36, 2012.
11) Ganju, A. et al.：Nanoways to overcome docetaxel resistance in prostate cancer. *Drug Resist. Updat.*, **17**：13-23, 2014.
12) Sato, A. et al.：Magnetic nanoparticles of Fe3O4 enhance docetaxel-induced prostate cancer cell death. *Int. J. Nanomed.*, **8**：3151-3160, 2013.
13) 一町直樹・他：各種ナノ粒子の細胞への影響：細胞特異性とその応用．粉体工学会誌，**48**：25-31，2011.
14) Khanrika, L. et al.：Oxidative stress in prostate cancer. *Cancer Lett.*, **282**：125-36, 2009.
15) Torres-Lugo, M. et al.：Thermal potentiation of chemotherapy by magnetic nanoparticles. *Nanomedicine*, **8**：1689-1707, 2013.

*　　*　　*

adfm201504215(201504215)

www.afm-journal.de

ADVANCED FUNCTIONAL MATERIALS

Smart Ferrofluid with Quick Gel Transformation in Tumors for MRI-Guided Local Magnetic Thermochemotherapy

By *Koichiro Hayashi,* Wataru Sakamoto, and Toshinobu Yogo*

Keywords: drug delivery, ferrofluid, hyperthermia, magnetic resonance imaging, theranostics

Improved techniques for local administration of anticancer drugs are needed to reduce the side effects of chemotherapy owing to leakage of anticancer drugs from tumors and to enhance therapeutic efficacy. This study presents the development of smart ferrofluid that transforms immediately into a gel in tumors and generates heat in response to an alternating magnetic field (AMF), simultaneously releasing the anticancer drug. The smart ferrofluid, which is synthesized using less toxic magnetic materials (Fe_3O_4 nanoparticles), natural polysaccharides (alginate), and amino acids (cysteine), can also act as a contrast agent for magnetic resonance imaging (MRI). The ferrofluid also incorporates an anticancer drug (i.e., doxorubicin, DOX) via hydrogen bonds. AMF causes heating of gels prepared from the DOX-containing ferrofluid, resulting in gel shrinkage and DOX release. In vivo experiments demonstrated that the ferrofluid transforms into a gel in the tumor, with the gel remaining in the tumor. Furthermore, magnetic thermochemotherapy using this ferrofluid inhibited tumor growth, while magnetic hyperthermia alone had only a marginal effect. Thus, the combination of magnetic hyperthermia and chemotherapy may be important for suppressing tumor growth. In summary, the ferrofluid presented here has the potential to facilitate MRI-guided magnetic thermochemotherapy through a combination of endoscopic technologies in the future.

1. Introduction

Magnetic hyperthermia is a new type thermotherapy that exploits the properties of magnetic nanoparticles, namely, generation of heat by hysteresis loss, Néel relaxation, and Brownian relaxation under the influence of an alternating magnetic field (AMF).[1–3] Magnetic hyperthermia may facilitate local treatment of deep tumors because heat is generated only in areas in which magnetic nanoparticles are present. Moreover, AMF can penetrate deeply into the body, providing the potential to target tumors in various organs. Current hyperthermia is often administered together with chemotherapy to enhance cancer treatment,[4] and magnetic hyperthermia can also improve the therapeutic efficacy of chemotherapy.

In practice, magnetic hyperthermia is performed by application of AMF to the body after direct administration of ferrofluid containing magnetic nanoparticles into the tumor.[1] Because direct administration of anticancer drugs into the affected area is routinely performed,[5–7] direct injection of ferrofluid into tumor may be technically feasible. However, when ferrofluid is administered directly into tumors, magnetic nanoparticles leak along the path of the needle (Figure S1a, Supporting Information). Furthermore, fluid leakage from the tumor can lead to accumulation of the magnetic nanoparticles in normal tissues around the tumor (Figure S1a, Supporting Information). As a result, when mice injected with the ferrofluid are exposed to AMF, normal tissues around the tumor rather than the tumor itself are heated (Figure S1b, Supporting Information). Therefore, effective local treatment using magnetic hyperthermia will require the development of novel methods to prevent the leakage of magnetic nanoparticles from the tumor.

This is also true for local chemotherapy; anticancer drugs are injected directly into tumors in local chemotherapy, but can leak from the tumor and pass into systemic circulation.[5,6] Therefore, techniques for local chemotherapy also need to be improved to ensure that the anticancer drugs remain in the tumor.

Current treatments for gastric tumors include endoscopic therapies, such as endoscopic mucosal resection (EMR) and en-

Dr. K. Hayashi, Dr. W. Sakamoto, Prof. T. Yogo, Division of Materials Research, Institute of Materials and Systems for Sustainability, Nagoya University, Furo-cho, Chikusa-ku Nagoya 464-8603, Japan
Correspondence to: Dr. K. Hayashi (E-mail: hayashi@esi.nagoya-u.ac.jp)
10.1002/adfm.201504215

ADVANCED FUNCTIONAL MATERIALS

www.afm-journal.de

doscopic submucosal dissection (ESD).[8,9] However, with these endoscopic therapies, cancer cells remain in tissues around the tumor excision site, such as the submucosa and muscularis propria, resulting in cancer recurrence and metastasis (Figure S2a–c, Supporting Information). In addition, these endoscopic therapies require technical expertise and can cause procedural complications, such as bleeding and perforation. In contrast, magnetic thermochemotherapy with ferrofluid may have the potential to destroy cancer cells, even those present in the submucosal layer, through injection into the submucosal layer using a syringe (Figure S2d, Supporting Information). Furthermore, magnetic resonance imaging (MRI)-guided magnetic thermochemotherapy with ferrofluid may be easily combined with current endoscopic therapies (Figure S2e, Supporting Information), and the combination of these techniques may be effective for preventing the recurrence and metastasis of cancer.

In this study, we developed a ferrofluid that transforms quickly into a gel to prevent leakage of magnetic nanoparticles and anticancer drug from the tumor. We also attempted local treatment of tumors with a combination of magnetic hyperthermia and chemotherapy, designated as magnetic thermochemotherapy, using our novel ferrofluid under the guidance of MRI.

2. Results and Discussion

2.1. Synthesis and Characterization

Considering the potential toxicity of the ferrofluid, we prepared water-based ferrofluid from Fe_3O_4 nanoparticles, which are used as an MRI contrast agent in clinical practice, a polysaccharide extracted from seaweed (alginate [ALG]), and an amino acid (cysteine), as shown in **Scheme 1**. We predicted that this fluid would transform into a gel in the tumor based on the following two facts: (1) ALG is ionically cross-linked with multivalent cations; and (2) biological bodies contain multivalent cations, such as Mg^{2+} and Ca^{2+} (Scheme 1b).

Fe_3O_4 nanoparticles generally settle out in aqueous solution. In our previous study, we found that modification of Fe_3O_4 nanoparticles with cysteine improved their dispersibility in water.[10] In addition, the cysteine immobilized on the surface of Fe_3O_4 nanoparticles may form hydrogen bonds with ALG, leading to uniform dispersion of Fe_3O_4 nanoparticles in ALG aqueous solution. Based on the above findings and expectations, we attempted to prevent the sedimentation of Fe_3O_4 nanoparticles by the modification of Fe_3O_4 nanoparticles with cysteine.

Cysteine-modified Fe_3O_4 nanoparticles (Cys-Fe_3O_4) were synthesized by the following two steps: (1) in situ synthesis of allyl-functionalized Fe_3O_4 nanoparticles (Allyl-Fe_3O_4) through the hydrolysis and condensation of iron (III) 3-allylacetylacetonate (IAA)[10–15]; and (2) modification of Fe_3O_4 nanoparticles by the thiol-ene click reaction between Allyl-Fe_3O_4 and cysteine.[10] This reaction progresses chemoselectively in high yield under all environmental conditions.

Next, Cys-Fe_3O_4 was mixed with ALG aqueous solution to prepare ferrofluid, designated as Cys-Fe_3O_4/ALG hybrid fluid.

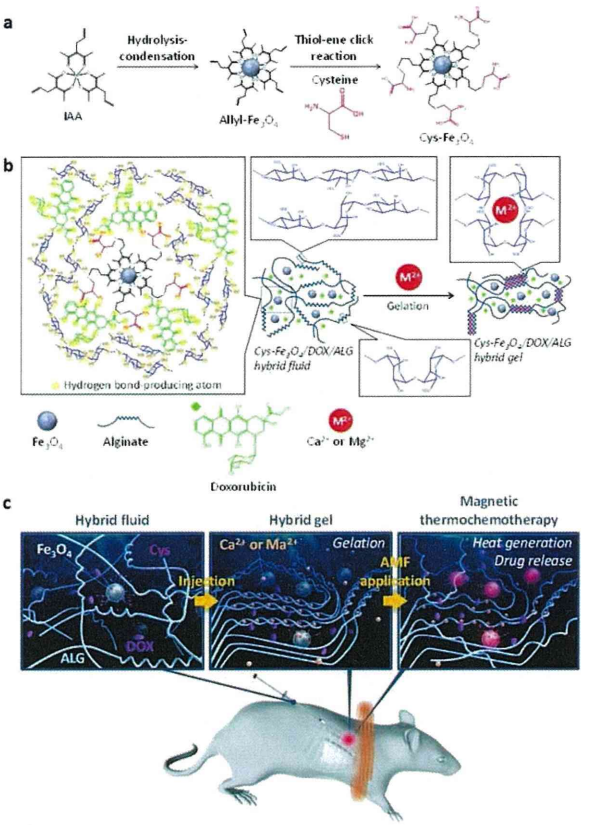

Scheme 1. a) Synthesis scheme for Cys-Fe_3O_4. b) Diagrammatic illustration of the transformation of Cys-Fe_3O_4/DOX/ALG hybrid fluid to hybrid gel. c) Illustration showing magnetic thermochemotherapy using Cys-Fe_3O_4/DOX/ALG hybrid fluid.

Using a similar method, we produced the ferrofluid consisted of Allyl-Fe_3O_4 and ALG aqueous solution, i.e., Allyl-Fe_3O_4/ALG hybrid fluid, as a control material. We compared the water dispersibilities of Cys-Fe_3O_4/ALG hybrid fluid and Allyl-Fe_3O_4/ALG hybrid fluid to assess the effects of the modification of Fe_3O_4 nanoparticles with cysteine on water dispersibility.

Furthermore, to achieve magnetic thermochemotherapy, we added the anticancer drug doxorubicin (DOX) to the above ferrofluids, designated as Cys-Fe_3O_4/DOX/ALG hybrid fluid and Allyl-Fe_3O_4/DOX/ALG hybrid fluid, respectively. DOX was easily incorporated into the Cys-Fe_3O_4/DOX/ALG hybrid fluid by simply mixing Cys-Fe_3O_4 and DOX-containing ALG aqueous solution because strong hydrogen bonds are formed between Cys-Fe_3O_4, DOX, and ALG. In contrast, Allyl-Fe_3O_4 does not form hydrogen bonds with DOX or ALG, exhibiting decreased DOX-holding ability and increased sedimentation of Fe_3O_4 nanoparticles.

The X-ray diffraction (XRD) pattern of Cys-Fe_3O_4 is coincident with that of Fe_3O_4 (JCPDS 01-088-0315), indicating the formation of Fe_3O_4 without byproducts (**Figure 1**a). The crystallite size of Fe_3O_4 nanoparticles calculated using the Scherrer

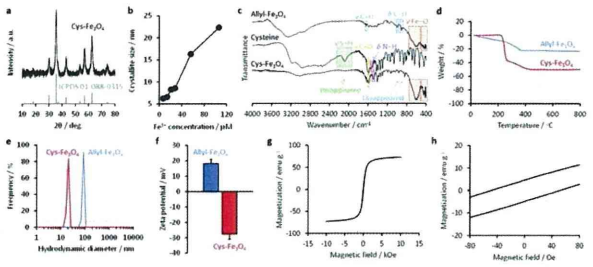

Figure 1. a) XRD patterns of Cys-Fe_3O_4 and Fe_3O_4 (JCPDS 01-088-0315). b) The relationship between the crystallite size and iron (III) ion concentration in precursor solution. c) FT-IR spectra of Allyl-Fe_3O_4, cysteine, and Cys-Fe_3O_4. d) TG curves of Allyl-Fe_3O_4 and Cys-Fe_3O_4. e) Particle size distribution and f) zeta potentials of Allyl-Fe_3O_4 and Cys-Fe_3O_4 in distilled water. g) Magnetization curve of Cys-Fe_3O_4. h) Magnified view of the origin in (g).

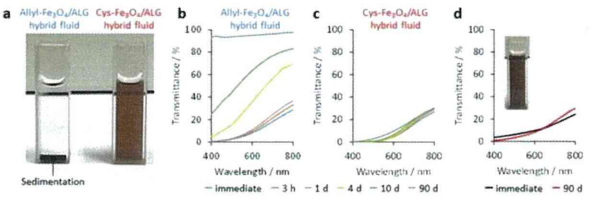

Figure 2. a) Photograph of Allyl-Fe_3O_4/ALG hybrid fluid and Cys-Fe_3O_4/ALG hybrid fluid 10 d after preparation. b) Transmission spectra of Allyl-Fe_3O_4/ALG hybrid fluid and c) Cys-Fe_3O_4/ALG hybrid fluid over time. d) Transmission spectra of Cys-Fe_3O_4/DOX/ALG hybrid fluid immediately and 90 d after preparation. A photograph of the hybrid fluid 90 d after preparation is shown in the inset.

formula is controllable by adjusting the concentration of iron (III) ions in precursor solution (Figure 1b). Our previous study revealed that Fe_3O_4 nanoparticles with a crystallite size of 16 nm had the maximum amount of heat generation.[12] As shown in Figure 1b, Fe_3O_4 nanoparticles had a crystallite size of 16 nm when the precursor solution had an iron (III) ion concentration of 56×10^{-6} M. The Fe_3O_4 nanoparticles were also about 16 nm in particle diameter, as shown by transmission electron microscopy (TEM; Figure S3, Supporting Information), indicating that their particle size was equal to their crystallite size. Accordingly, in this study, we used Fe_3O_4 nanoparticles measuring 16 nm.

In the FT-IR spectrum of Allyl-Fe_3O_4, the absorption bands attributable to the allyl group were observed at 1650 cm^{-1} (ν C=C), 995 cm^{-1} (δ C–H), and 910 cm^{-1} (δ C–H), as shown in Figure 1c. The spectrum of cysteine had an absorption band at 2075 cm^{-1} (ν S–H) due to the thiol group. The absorption bands attributed to the allyl and thiol groups disappeared in the spectrum of Cys-Fe_3O_4, demonstrating that the thiol-ene click reaction occurred between Allyl-Fe_3O_4 and cysteine. The spectrum of Cys-Fe_3O_4 also had these absorption bands due to Fe_3O_4 (ν Fe–O at 590 and 425 cm^{-1}) and cysteine (COO^- at 1590 cm^{-1} and NH_3^+ at 1485 cm^{-1}).[16] These findings confirmed that Fe_3O_4 nanoparticles were modified with cysteine through the thiol-ene click reaction between Allyl-Fe_3O_4 and cysteine.

Thermogravimetric (TG) curves showed that Allyl-Fe_3O_4 contained 16 wt% of organics, 77 wt% of Fe_3O_4, and 7 wt% of absorbed water, whereas Cys-Fe_3O_4 consisted of 50 wt% of organics and 50 wt% of Fe_3O_4 (Figure 1d). Thus, modification with cysteine increased the proportion of organics by 24 wt%, demonstrating that 2.0 mmol of cysteine is bound to the surface of the Fe_3O_4 nanoparticles per gram of Cys-Fe_3O_4.

The average hydrodynamic diameters of Allyl-Fe_3O_4 and Cys-Fe_3O_4, as measured by dynamic light scattering, were 87 and 20 nm, respectively, in distilled water (Figure 1e). The hydrodynamic diameter of Allyl-Fe_3O_4 was much larger than the particle size, indicating that Allyl-Fe_3O_4 aggregated in distilled water. On the other hand, Cys-Fe_3O_4 had a hydrodynamic diameter slightly larger than the particle size. Thus, modification with cysteine enhanced the dispersibility of the nanoparticles in distilled water and prevented aggregation. In addition, the zeta potentials of Allyl-Fe_3O_4 and Cys-Fe_3O_4 were 18 and –28 mV, respectively (Figure 1f); the change in zeta potential from positive to negative further confirmed that cysteine is bound to the Fe_3O_4 nanoparticles.

Cys-Fe_3O_4 exhibited a hysteresis loop at room temperature due to the inherent magnetic properties (i.e., ferrimagnetism) of Fe_3O_4 (Figure 1g,h). The saturation magnetization, remanent magnetization, and coercivity were 73 emu g^{-1}, 5 emu g^{-1}, and 50 Oe, respectively.

2.2. Dispersivity in Water

To evaluate the effects of the modification of Fe_3O_4 nanoparticles with cysteine on the water dispersivity, we measured the transmittance of Fe_3O_4/ALG hybrid fluid and Cys-Fe_3O_4/ALG hybrid fluid. Allyl-Fe_3O_4 gradually settled out (**Figure 2**a), resulting in an increase in the transmittance of Allyl-Fe_3O_4/ALG hybrid fluid with time (Figure 2b). On the other hand, Cys-Fe_3O_4/ALG hybrid fluid showed minor changes in transmittance over at least a 90 d period (Figure 2c) because Cys-Fe_3O_4 remained dispersed in the fluid, even after 90 d (Figure 2a). These results demonstrated that the modification of Fe_3O_4 nanoparticles with cysteine enhanced the water dispersibility of the nanoparticles. Generally, nanoparticles are coated with dextran, citrate, or other molecules to enhance their dispersibility in water. However, these agents merely coat nanoparticles and can be easily removed. In contrast, cysteine can link covalently to Fe_3O_4 nanoparticles by the thiol-ene click reaction. Furthermore, cysteine can form strong hydrogen bonds with both ALG and DOX. Considering these advantages of cysteine over common coating agents, we used cysteine to enhance both the water dispersibility of the nanoparticles and the DOX-holding ability of the gel, as described in Section 2.4.

We also investigated the stability of the Cys-Fe_3O_4/DOX/ALG hybrid fluid by measuring the transmittance immediately and at 90 d after preparation. There were no major differences in the transmittance at either time point (Figure 2d), indicating that the hybrid fluid remained stable for at least 3 months.

ADVANCED FUNCTIONAL MATERIALS

www.afm-journal.de

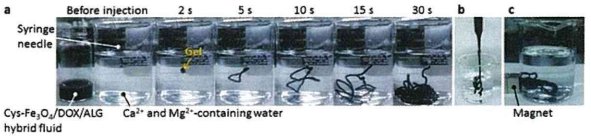

Figure 3. a) Photographs showing the gelation of Cys-Fe_3O_4/DOX/ALG hybrid fluid by injection into Ca^{2+}- and Mg^{2+}-containing water, b) lifting of Cys-Fe_3O_4/DOX/ALG hybrid gel with tweezers, and c) magnetic guidance of Cys-Fe_3O_4/DOX/ALG hybrid gel.

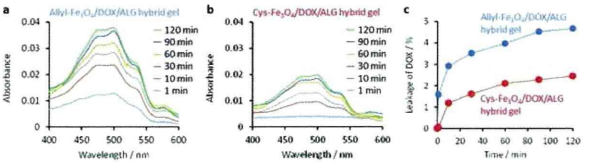

Figure 4. a) Absorption spectra of supernatants collected from PBS containing Allyl-Fe_3O_4/DOX/ALG hybrid gel and b) Cys-Fe_3O_4/DOX/ALG hybrid gel without the influence of AMF. c) Changes in the fraction of DOX released from the Allyl-Fe_3O_4/DOX/ALG hybrid gel and Cys-Fe_3O_4/DOX/ALG hybrid gel over time.

2.3. In Vitro Gelation

To simulate the gelation of Cys-Fe_3O_4/DOX/ALG hybrid fluid in tumors, we injected the hybrid fluid into aqueous solution containing Mg^{2+} and Ca^{2+} at a concentration equal to that in extracellular fluid. This hybrid fluid turned into a gel immediately after contacting the aqueous solution (**Figure 3**a; Movie S1, Supporting Information). The gel could be picked up with tweezers (Figure 3b) and responded to a magnet (Figure 3c).

2.4. Drug-Holding Ability

To investigate the DOX-holding abilities of Allyl-Fe_3O_4/DOX/ALG hybrid gel and Cys-Fe_3O_4/DOX/ALG hybrid gel, the hybrid gels were immersed in phosphate-buffered saline (PBS) without application of AMF, and the absorbance due to DOX in the supernatant was then measured over time (**Figure 4**a,b). The solution containing the Allyl-Fe_3O_4/DOX/ALG hybrid gel showed higher absorbance in the supernatant than that containing the Cys-Fe_3O_4/DOX/ALG hybrid gel. After 120 min, the absorbance of the solution containing the Allyl-Fe_3O_4/DOX/ALG hybrid gel was twice as large as that containing the Cys-Fe_3O_4/DOX/ALG hybrid gel. The leakage of DOX from these hybrid gels was estimated by the Beer–Lambert law using the absorbance. From this analysis, the leakage of DOX from the Allyl-Fe_3O_4/DOX/ALG hybrid gel was 4.7% and that from the Cys-Fe_3O_4/DOX/ALG hybrid gel was 2.4% (Figure 4c). Thus, the Cys-Fe_3O_4/DOX/ALG hybrid gel had a twofold greater DOX-holding ability than the Allyl-Fe_3O_4/DOX/ALG hybrid gel owing to the modification of Fe_3O_4 nanoparticles with cysteine, which enhanced the hydrogen bonds within the hybrid gel to prevent leakage of DOX. The results in Figures 2 and 4 demonstrated that modification of Fe_3O_4 nanoparticles with cysteine was effective for both the prevention of sedimentation of the Fe_3O_4 nanoparticles and for enhancement of DOX-holding ability.

2.5. Heat Generation Power

Next, we investigated the exothermal behavior of Cys-Fe_3O_4/DOX/ALG hybrid gels prepared from the hybrid fluid containing Fe_3O_4 at a concentration of 4 mg mL^{-1}. **Figure 5**a shows thermal images of the hybrid gel under the influence of AMF with a frequency (f) of 217 kHz and a magnetic field (H) of 8 kA m^{-1} ($Hf = 1.7 \times 10^9$ A m^{-1} s^{-1}); AMF with an Hf value of less than 5×10^9 A m^{-1} s^{-1} is considered to be harmless.[17] The hybrid gel generated heat immediately after application of AMF (Figure 5a,b). The specific loss power (SLP) of the hybrid gel was 495 W g^{-1} (see the Experimental Section). More importantly, the hybrid gel exhibited a dramatic increase in temperature after 6 min of AMF application (Figure 5b) and simultaneously shrunk (Figure 5a,c). To elucidate the mechanism mediating the shrinkage of the hybrid gel, we measured water content in the hybrid gel before and after the application of AMF using differential thermal analysis-thermogravimetry (DTA-TG). The hybrid gel contained 93 wt% water before the application of AMF (Figure 5d). After exposure to AMF for 10 min, the water content was decreased by 82–11 wt%. Scanning electron microscope (SEM) images also showed that the hybrid gel had a rough surface and pores after exposure to AMF, indicating that heat generation in the hybrid gel depleted the water contained within the gel (Figure 5e,f). These findings demonstrated that the hybrid gel generated an enormous amount of heat under AMF to evaporate the contained water, resulting in the shrinkage of the hybrid gel. The decrease in water content also facilitated the thermal elevation of the hybrid gel, resulting in a dramatic increase in the temperature of the hybrid gel after 6 min of AMF application. This consideration is also supported by the comparison in exothermic behaviors between the fluid state and the gel state. The temperature of the hybrid fluid increased by 42 °C in 10 min (Figure S4a,b, Supporting Information), which was approximately equal to temperature increase of the hybrid gel at 5–6 min (by 38–48 °C). In addition, the SLP of the hybrid fluid was 122 W g^{-1}, which was about a quarter of that in the hybrid gel. However, water in the hybrid fluid was evaporated by exposure to AMF; water droplets adhered to the wall surface of the glass vial (Figure S4c, Supporting Information) so that the derived SLP for the gel was overestimated compared with the hybrid fluid. This result suggested that there were no differences in the heat generation power of Fe_3O_4 nanoparticles between the hybrid fluid and hybrid gel. Thus, the differences in temperature increases between the hybrid fluid and hybrid gel could be explained in two ways. First, the fraction of surface in the gel system was significantly larger than that of the water surface in the fluid system. Therefore, water contained in the hybrid gel could be more easily removed from the system than water in the hybrid fluid. Second, the hybrid fluid was sealed in a vial. Therefore, cooled water droplets returned to the hybrid fluid. The above findings supported that the removal of water from the hybrid

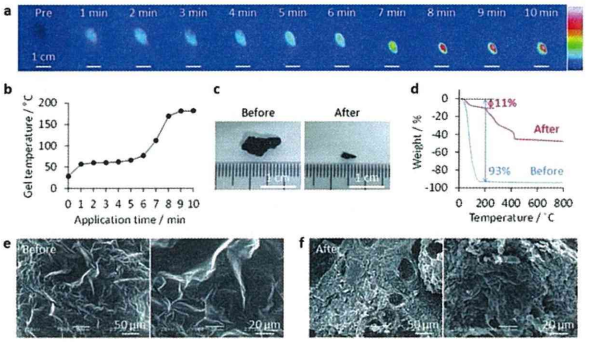

Figure 5. a) Thermal images of the Cys-Fe_3O_4/DOX/ALG hybrid gel under the influence of AMF. b) Changes in gel temperature with AMF application time. c) Photographs and d) TG curves of Cys-Fe_3O_4/DOX/ALG hybrid gel before and 10 min after AMF application. SEM images of Cys-Fe_3O_4/DOX/ALG hybrid gel e) before and f) 10 min after of AMF application.

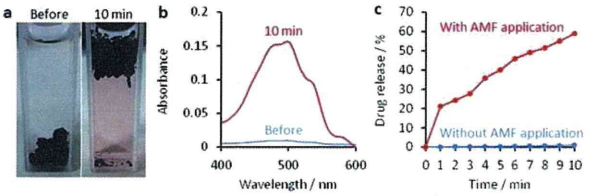

Figure 6. a) Photographs of PBS containing the Cys-Fe_3O_4/DOX/ALG hybrid gel before AMF application and after 10 min of AMF application. b) Absorption spectra of supernatants collected from PBS containing the Cys-Fe_3O_4/DOX/ALG hybrid gel before and 10 min after AMF application. c) Proportion of DOX released from the Cys-Fe_3O_4/DOX/ALG hybrid gel with and without AFM application.

gel caused a dramatic increase in the temperature of the hybrid gel after 6 min of AMF application.

2.6. Drug Release

The remotely controlled release of DOX using AMF as a trigger could be achieved by exploiting the shrinkage phenomenon of the Cys-Fe_3O_4/DOX/ALG hybrid gel. To estimate the rate of released DOX, the hybrid gel was immersed in PBS and then subjected to AMF for 10 min. The supernatant turned slightly pink after AMF application for 10 min (**Figure 6**a). The absorption spectra showed absorbance due to DOX increased in the supernatant after AMF application (Figure 6b). These findings confirmed that the hybrid gel released DOX in response to AMF. Furthermore, the hybrid gel floated after AMF application, as shown in Figure 6a, because it released contents such as DOX and water, resulting in weight loss and the formation of pores (see Figure 5f). This result confirmed that the hybrid gel released DOX along with the contained water following exposure to AMF. The release rate of DOX was estimated by the Beer–Lambert law using the absorbance due to DOX in the supernatant. From this analysis, we found that the hybrid gel released significant amounts of DOX following application of AMF, whereas little DOX was released without AMF: the fractions of released DOX with and without AMF were 61.5% and 1.2%, respectively (Figure 6c). One hundred twenty minutes after immersing the hybrid gel in PBS, the leakage of DOX from the hybrid gel was 2.4%, as shown in Figure 4c. These results indicated that the hybrid gel enabled the systematic release of DOX using AMF as a trigger.

2.7. In Vivo Gelation

Previous studies by Le Renard et al. described an injectable hydrogel for magnetic hyperthermia.[18,19] This hydrogel could not be applied to magnetic hyperthermia because magnetic particles were not tightly incorporated in the hydrogel, and the fraction of magnetic particles was insufficient in the tumor. Based on these results, we enhance the interaction of magnetic nanoparticles with each component in the ferrofluid by forming hydrogen bonding, as described above. Chen et al. reported an injectable organogel that could be used for magnetic hyperthermia.[20] The organogel contained *N*-methylpyrrolidone as medium; this component is toxic to skin and respiratory organs and can cause cancer, adverse effects on reproductive competence and fetal develop, and damage to the spleen, liver, kidney, respiratory organs, bone marrow, and adrenal glands.[21,22] Accordingly, the ferrofluid produced in this study was designed using only nontoxic materials, which would facilitate their application in preclinical models.

Injectable gels, including those containing chitosan, poly(*N*-isopropylacrylamide), and block copolymers, can also be used as carriers for local drug delivery, with changes in temperature and pH used as triggers for controlled drug release.[23–25] However, the use of exogenous physical stimuli, including light,[26] ultrasound,[27] and electric current,[28] as the trigger enables remote and externally regulated controlled drug release. In this study, we used AMF as the trigger because it can penetrates deep into the body.[29] In addition, we used MRI to confirm the formation and localization of the gel; this method, like ultrasound,[30–32] X-ray,[31–33] and fluorescence imaging techniques,[34] is noninvasive and also provides high spatial resolution.[32]

Based on this rational development process, we next sought to realize safe and effective magnetic thermochemotherapy. Therefore, we confirmed that the ferrofluid transformed into gel in the tumor and that the gel localized in the tumor using MRI. We injected Cys-Fe_3O_4/DOX/ALG hybrid fluid subcutaneously into the backs of normal mice and then excised the subcutaneous tissue at the site of administration. The gel formed on the excised subcutaneous tissue, as shown in **Figure 7**a. To establish that the hybrid gel remained in the tumor, we injected the hybrid fluid intratumorally into mice bearing subcutaneous xenograft tumors derived from HGC-27 gastric cancer cells at multiple sites. As shown in T2-weighted MR images (Figure 7b), the MRI signal of the tumor was locally reduced after injection of the hybrid fluid. To confirm the gelation of the hybrid fluid within the tumor, we excised the tumors from mice after MRI and cut the tumors in half lengthwise. Photographs of

ADVANCED FUNCTIONAL MATERIALS

the halved tumors revealed that the hybrid fluid transformed into a gel within the tumor, as shown in Figure 7c. Additionally, Figure 7f shows hematoxylin and eosin (HE)-stained and iron-stained tumor sections and fluorescence images of unstained tumor sections following injection of the hybrid fluid. Iron staining revealed that abundant Fe_3O_4 nanoparticles were present in the tumor. Furthermore, fluorescence images of unstained sections revealed that DOX was located adjacent to Fe_3O_4 nanoparticles. The above findings demonstrated that the Cys-Fe_3O_4/DOX/ALG hybrid fluid transformed into a gel immediately after injection into the tumor and that the hybrid gel remained in the tumor (Figure 7a–c,f). In addition, these findings indicated that monitoring with noninvasive MRI provided conclusive evidence that the hybrid fluid transformed into a gel and localized in the tumor without invasive evaluation or dissection.

2.8. In Vivo Therapeutic Efficacy

To investigate the therapeutic efficacy of magnetic thermochemotherapy using Cys-Fe_3O_4/DOX/ALG hybrid fluid, we injected the hybrid fluid intratumorally into tumor-bearing mice. Shortly thereafter, we applied AMF to mice under anesthesia for 20 min. For comparison, we prepared the following control groups: untreated mice, mice exposed to AMF alone, mice subjected to intratumoral administration of Cys-Fe_3O_4/DOX/ALG hybrid fluid, mice subjected to intratumoral administration of DOX (chemotherapy alone), and mice exposed to AMF after intratumoral administration of Cys-Fe_3O_4/ALG hybrid fluid (magnetic hyperthermia alone). The dosage of DOX was equivalent to the clinical dose of DOX applied in patients with gastric cancer. The above hybrid fluids and DOX were injected into multiple sites within the tumors. AMF was applied just once at the start of the measurement period.

AMF application after the administration of Cys-Fe_3O_4/DOX/ALG hybrid fluid heated the tumor locally by about 10 °C in 20 min (Figure 7d,e). On the other hand, AMF application alone did not increase tumor temperature; a decrease in tumor temperature was actually observed because of the influence of anesthesia (Figure 7e).

We investigated the diffusion behaviors of DOX released from the hybrid gel in the tumor by histological analyses. DOX was only found adjacent to Fe_3O_4 nanoparticles following injection of hybrid fluid (Figure 7f), whereas DOX spread to locations distant from Fe_3O_4 nanoparticles and that were lacking Fe_3O_4 nanoparticles, as indicated by yellow triangles, 24 h after AMF application (Figure 7g). These findings revealed that DOX was released from the hybrid gel by AMF application, spread throughout the tumor, and remained in the tumor for 24 h after AMF removal. Thus, DOX continued to affect the tumor over a long period of time. Ten days after treatment, the amounts of Fe_3O_4 nanoparticles and DOX in the tumor decreased (Figure 7h). However, some residual ferrofluid and DOX remained in the tumor, indicating the gradual breakdown of hybrid gel.

Next, we estimated the therapeutic efficacy of the treatment based on the change in tumor volume (**Figure 8**c). Chemotherapy alone had no effect on treatment. This may be explained by the administration of only a single dose of DOX and the leakage

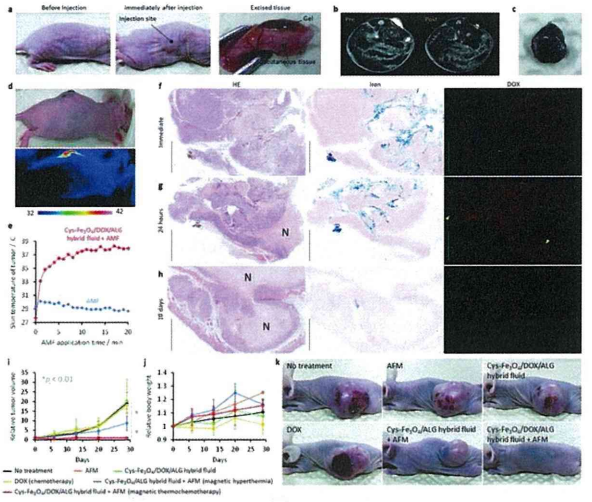

Figure 7. a) Photographs of mice before and immediately after injection of Cys-Fe_3O_4/DOX/ALG hybrid fluid and excised tissue at the site of administration (left to right). b) MR images of tumor-bearing mice before and immediately after injection of Cys-Fe_3O_4/DOX/ALG hybrid fluid. Yellow circles indicate tumor sites. c) Photograph of a representative tumor halved lengthwise. The tumor was excised from mice immediately after injection of the hybrid gel. d) Photograph and thermal image of tumor-bearing mice injected with the Cys-Fe_3O_4/DOX/ALG hybrid fluid under the influence of AMF. e) Changes in the skin temperatures of tumors over time after AMF application. Mice injected with Cys-Fe_3O_4/DOX/ALG hybrid fluid (red) and untreated mice (blue). Tumor sections from mice f) before and g) 24 h or h) 10 d after injection of Cys-Fe_3O_4/DOX/ALG hybrid fluid: HE staining (left), iron staining (middle), and fluorescence image of unstained sections (right). Scale bars indicate 5 mm. N: necrotic tissue. Blue-stained regions indicate the presence of Fe_3O_4 nanoparticles in the iron-stained section. Yellow triangles indicate the locations of DOX distant from Fe_3O_4 nanoparticles and that are lacking Fe_3O_4 nanoparticles. Red fluorescence regions indicate the presence of DOX in the fluorescence image of unstained sections. Changes in i) relative tumor volumes and j) relative body weights over time. k) Photographs of mice 29 d after treatment.

of DOX from the tumor. Indeed, anticancer drugs are known to be able to leak from the tumor and pass into systemic circulation if injected directly into tumors for local chemotherapy.[5,6] Magnetic hyperthermia alone inhibited tumor growth to some degree. However, magnetic thermochemotherapy markedly inhibited tumor growth and showed significantly greater therapeutic efficacy than magnetic hyperthermia alone. There were no significant differences in body weights between all groups (Figure 7j). Photographs of mice at 29 d after treatment also showed that magnetic thermochemotherapy obviously inhibited tumor growth (Figure 7k). The above results demonstrated that magnetic thermochemotherapy had greater therapeutic effects than chemotherapy alone or magnetic hyperthermia alone. This may be explained by the observation that magnetic

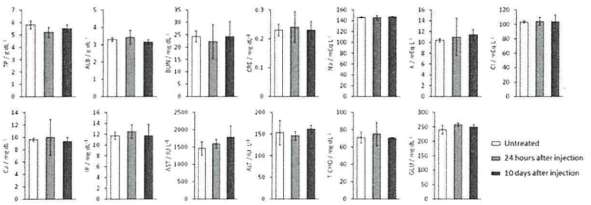

Figure 8. Biochemical assays in the sera of mice 24 h and 10 d after injection of the hybrid fluid and untreated mice: total protein (TP), albumin (ALB), blood urea nitrogen (BUN), creatinine (CRE), sodium, potassium, chloride, calcium, inorganic phosphate (IP), aspartic aminotransferase (AST), alanine aminotransferase (ALT), total cholesterol (T-CHO), and glucose (GLU).

hyperthermia alone heated and destroyed a small portion of the tumor because Fe_3O_4 nanoparticles were heterogeneously located in the tumor, as shown in Figure 7f. In contrast, in magnetic thermochemotherapy, DOX spread to areas in which Fe_3O_4 nanoparticles were not present (i.e., areas where the hybrid gel did not heat), as shown in Figure 7g, damaging a wider range of the tumor area. In fact, the tumor tissues necrotized, even in areas in which Fe_3O_4 nanoparticles were absent (Figure 7g,f). Furthermore, the prolonged presence of DOX in the tumor realized continuous chemotherapy and contributed to the enhancement of therapeutic efficacy.

Thus, from these in vivo studies, we were able to achieve MRI-guided magnetic thermochemotherapy with the ferrofluid as follows: (1) the ferrofluid incorporated the anticancer drug through hydrogen bonding between the ferrofluid and anticancer drug; (2) the ferrofluid transformed into a gel immediately after injection into tumors in mice; (3) MRI allowed visualization of the gelation of the ferrofluid in the tumor and localization of the gel; (4) when tumor-bearing mice injected with the ferrofluid were exposed to AMF, the gel formed in the tumor generated heat in response to AMF, achieving magnetic hyperthermia; and (5) the gel shrank in response to heat generation, resulting in the release of the anticancer drug from the gel. Thus, chemotherapy was achieved at the same time as magnetic hyperthermia.

2.9. In Vivo Toxicity

Finally, the toxicity of the hybrid fluid at 24 h and 10 d after injection was evaluated by biochemical assays using sera from mice (Figure 9). The DOX-treated mice exhibited significantly higher levels of calcium, inorganic phosphate (IP), aspartic aminotransferase (AST), alanine aminotransferase (ALT), and total cholesterol (T-CHO) and lower levels of total protein (TP), sodium, chloride, and glucose (GLU) compared with those in untreated mice resulting from the disorders of the liver, kidneys, endocrine system, carbohydrate metabolism, water metabolism, and bone metabolism (Figure S5, Supporting Information). These effects may be explained by the entry of DOX into systemic circulation immediately after injection. In contrast, there were no significant differences in the levels of TP, albumin (ALB), blood urea nitrogen (BUN), creatinine (CRE), sodium, potassium, chloride, calcium, IP, AST, ALT, T-CHO, and GLU between untreated mice and treated mice at 24 h and 10 d after injection of the hybrid fluid. Thus, the hybrid fluid had no significant toxicities in mice within 10 d after injection. Histological findings (Figure 7f–h) also suggested that the hybrid gel had no significant toxicities because DOX did not pass into systematic circulation immediately after injection owing to the slow spread of DOX released from the hybrid gel and the retention of DOX in the tumor over a prolonged period of time (for at least 24 h). Furthermore, most of the hybrid gel broke down within 10 d.

3. Conclusion

In this study, we successfully synthesized smart ferrofluid that transformed into a gel immediately after injection into tumors using biocompatible materials. The hydrogen bonds within the ferrofluid enhanced both the dispersibility of the Fe_3O_4 nanoparticles and the DOX-holding ability of the gel. The Cys-Fe_3O_4/DOX/ALG hybrid gel generated heat in response to AMF. At the same time, the gel shrank, releasing DOX. Cys-Fe_3O_4/DOX/ALG hybrid fluid transformed into a gel within the tumor immediately after injection into tumor-bearing mice under the guidance of MRI. Application of AMF to mice injected with Cys-Fe_3O_4/DOX/ALG hybrid fluid heated the tumor locally. Thus, magnetic thermochemotherapy using the Cys-Fe_3O_4/DOX/ALG hybrid fluid showed significantly greater therapeutic efficacy than chemotherapy alone or magnetic hyperthermia alone. The hybrid fluid had significantly lower toxicity than DOX alone.

4. Experimental Section

Materials: IAA was prepared as previously described.[35] Hydrazine hydrate was purchased from Kishida Chemical Co., Ltd. (Osaka, Japan). Sodium alginate (ALG; 300–400 cP) and 2,2′-azobis[2-(2-imidazolin-2-yl)propane]dihydrochloride (AIPD) were purchased from Wako Pure Chemical Industries, Ltd. (Osaka, Japan). Cysteine and DOX were purchased from Tokyo Chemical Industry Co., Ltd. (Tokyo). These reagents were used as received.

Synthesis of Allyl-Fe_3O_4: IAA was dissolved in ethanol at various concentrations (7–106 $\times$ 10^{-3} M).[10–15] Hydrazine hydrate (70 equiv. to IAA) and distilled water (200 equiv. to IAA) were added to the IAA solution at room temperature. The mixed solution was then heated at 80 °C for 24 h. The products were collected by centrifugation at 15 000 rpm for 20 min and were then redispersed in distilled water. This processing was repeated at least three times to wash the products.

Synthesis of Cys-Fe_3O_4: Allyl-Fe_3O_4 nanoparticles were dispersed in distilled water at a concentration of 6 mg mL^{-1}.[10] Cysteine (10×10^{-6} M) and AIPD (10×10^{-6} M) were added to the aqueous dispersion containing Allyl-Fe_3O_4, and the mixture was stirred at 40 °C for 24 h. The product was collected by centrifugation at 15 000 rpm for 20 min and then redispersed

ADVANCED FUNCTIONAL MATERIALS

in distilled water. This processing was repeated at least three times to wash the product.

Preparation of Allyl-Fe_3O_4/ALG Hybrid Fluid and Cys-Fe_3O_4/ALG Hybrid Fluid: The aqueous dispersions of Allyl-Fe_3O_4 or Cys-Fe_3O_4 (2 mg mL^{-1}, 5 mL), designated as Allyl-Fe_3O_4/ALG hybrid fluid and Cys-Fe_3O_4/ALG hybrid fluid, respectively, were mixed with ALG aqueous solution (20 mg mL^{-1}, 2 mL) using a vortex mixer for 30 s.

In Vitro Gelation of Allyl-Fe_3O_4/DOX/ALG Hybrid Fluid and Cys-Fe_3O_4/DOX/ALG Hybrid Fluid: DOX (1.2 mg) was dissolved in the aqueous dispersions of Allyl-Fe_3O_4 or Cys-Fe_3O_4 (6 mg mL^{-1}, 5 mL). The dispersions were mixed with ALG aqueous solution (20 mg mL^{-1}, 2 mL) using a vortex mixer for 30 s to obtain fluids consisting of Allyl-Fe_3O_4 or Cys-Fe_3O_4, DOX, and ALG hybrid fluids, which were designated as Allyl-Fe_3O_4/DOX/ALG hybrid fluid and Cys-Fe_3O_4/DOX/ALG hybrid fluid, respectively. $CaCl_2$ and $MgCl_2$ were dissolved in distilled water; the concentrations of Ca^{2+} and Ma^{2+} were 1.8×10^{-3} and 1.5×10^{-3} M, respectively, similar to the concentrations of these ions in the extracellular fluid. The above hybrid fluids were injected into the Ca^{2+}- and Mg^{2+}-containing aqueous solutions. As a result, these hybrid fluids transformed into the gel state. The gels prepared from Allyl-Fe_3O_4/DOX/ALG hybrid fluid and Cys-Fe_3O_4/DOX/ALG hybrid fluid were designated as Allyl-Fe_3O_4/DOX/ALG hybrid gel and Cys-Fe_3O_4/DOX/ALG hybrid gel, respectively.

Structural Analysis and Magnetic Properties: The crystalline phases of Allyl-Fe_3O_4 and Cys-Fe_3O_4 were analyzed by X-ray diffraction (Rigaku SmartLab; Rigaku, Tokyo, Japan). The crystallite size was estimated using (311) reflection of Fe_3O_4 based on the Scherrer equation. The FT-IR spectra of cysteine, Allyl-Fe_3O_4, and Cys-Fe_3O_4 were recorded with an FT-IR spectrometer (Nexus 470; Nicolet, Madison, WI, USA). The amounts of inorganic and organic phases of Allyl-Fe_3O_4, Cys-Fe_3O_4, and Cys-Fe_3O_4/DOX/ALG hybrid gel were measured using DTA-TG (TG 8120, Rigaku). The size and shape of Cys-Fe_3O_4 nanoparticles were observed using TEM (H-800; Hitachi, Tokyo, Japan). The magnetic properties of Cys-Fe_3O_4 nanoparticles were measured with a vibrating sample magnetometer (VSM-C7-10A; Toei Kogyo, Tokyo, Japan) at room temperature.

Dispersibilities of Allyl-Fe_3O_4 and Cys-Fe_3O_4 in Water: The Allyl-Fe_3O_4/ALG hybrid fluid and Cys-Fe_3O_4/ALG hybrid fluid (1.2 mL) were diluted with distilled water (2.0 mL). To investigate the dispersibilities of Allyl-Fe_3O_4 and Cys-Fe_3O_4 in water, the optical transmittances of the diluted hybrid fluids were measured over time using an ultraviolet–visible (UV–vis) spectrophotometer (V-570; JASCO, Tokyo, Japan).

DOX Leakage from the Allyl-Fe_3O_4/DOX/ALG Hybrid Gel and Cys-Fe_3O_4/DOX/ALG Hybrid Gel without Application of AMF: Allyl-Fe_3O_4/DOX/ALG hybrid fluid and Cys-Fe_3O_4/DOX/ALG hybrid fluid (1 mL) were added to an aqueous solution containing Ca^{2+} and Mg^{2+} (4 mL) to prepare Allyl-Fe_3O_4/DOX/ALG hybrid gel and Cys-Fe_3O_4/DOX/ALG hybrid gel; both types of gels contained 0.18 mg DOX each. The hybrid gels were then placed in PBS. The DOX released from these hybrid gels was detected by measuring the absorbance of the supernatants using a UV-Vis spectrophotometer.

Heat Generation Powers of the Cys-Fe_3O_4/DOX/ALG Hybrid Fluid and the Cys-Fe_3O_4/DOX/ALG Hybrid Gel: The Cys-Fe_3O_4/DOX/ALG hybrid fluid and the Cys-Fe_3O_4/DOX/ALG hybrid gel were placed in the center of the coil and then exposed to AMF with a frequency (f) of 217 kHz and a magnetic field (H) of 8 kA m^{-1} ($Hf = 1.7 \times 10^9$ A m^{-1} s^{-1}). Both the hybrid fluid and hybrid gel contained 4 mg mL^{-1} Fe_3O_4. The temperatures of the hybrid fluid and hybrid gel were monitored using an infrared thermography camera (Thermo Gear G100EX; NEC Avio Infrared Technologies, Tokyo, Japan). The SLP was calculated as follows

$$\mathrm{SLP}\,(W/g) = c\,(M/m)\,(\mathrm{d}T/\mathrm{d}t)$$

where c is the heat capacity of water, M is the mass of the hybrid fluid or hybrid gel, m is the mass of the Fe_3O_4 in the hybrid gel or the hybrid fluid, and $\mathrm{d}T/\mathrm{d}t$ is the slope for the first 1 min in the heating curve.[36]

DOX Release from the Cys-Fe_3O_4/DOX/ALG Hybrid Gel with Application of AMF: The Cys-Fe_3O_4/DOX/ALG hybrid gel was placed in a quartz cell filled with PBS. The quartz cell was placed in the center of coil and exposed to AMF with a frequency f of 217 kHz and a magnetic field H of 8 kA m^{-1}. To estimate the amount of DOX released from the hybrid gels, the absorbance of the supernatant was measured over time using a UV–vis spectrometer. The amount of DOX released from the hybrid gels was calculated by the Beer–Lambert law, using the equation $A = \varepsilon CL$, where A is the absorbance of the supernatant at a wavelength of 495 nm, ε is the molar absorbance coefficient of DOX (10410 M^{-1} cm^{-1}), C is the molar concentration of DOX in the supernatant, and L is the length of light path (1 cm).

Cell Line and Animals: HGC-27 human gastric cancer cells were obtained from RIKEN Cell Bank. Cells were maintained in DMEM (Sigma, St. Louis, MO, USA) containing fetal bovine serum (Gibco) in a humidified atmosphere containing 5% CO_2 at 37 °C. BALB/c-nu/nu mice (female; 4 weeks of age) were purchased from Japan SLC (Shizuoka, Japan) and were maintained in a specific pathogen-free facility in the Center for Animal Research and Education of Nagoya University. All animal experiments were conducted with the approval of the Animal Care Committee of Nagoya University and were in accordance with the Fundamental Academic Research Institution in Japan. Inoculation of HGC-27 cells (3×10^6 cells per animal) was carried out by subcutaneous injection into the backs of the mice.

In Vivo Gelation of Cys-Fe_3O_4/DOX/ALG Hybrid Fluid: The Cys-Fe_3O_4/DOX/ALG hybrid fluid (containing 1.5 mg mL^{-1} Fe_3O_4; total dosage: 0.2 mL per mouse) was injected subcutaneously into the backs of normal BALB/c-nu/nu mice. Shortly thereafter, we excised the subcutaneous tissue at the site of injection to confirm the formation of the gel visually.

In Vivo MRI: The T2-weighted MR images of tumor-bearing mice were acquired before and immediately after intratumoral injection of the hybrid fluid at multiple sites (4 mg mL^{-1} Fe_3O_4; total dosage: 0.1 mL/mouse) using a compact MRI system (MR-mini SA; DS Pharma Biomedical, Osaka, Japan). The parameters were set as follows: TR = 2000; TE = 69 ms; thickness = 1.5 mm; and number of averages = 2.

Histological Analyses: The tumor was excised after taking MR images and immediately immersed in 4% paraformaldehyde at 4 °C for 48 h. Fixed tissues were encased in paraffin blocks and sectioned to a thickness of 2 μm. HE and iron staining of tissue sections were carried out using standard methods. The